First-order reflection/transmission coefficients for unconverted plane P waves in weakly anisotropic media

Véronique Farra, Ivan Pšenčík

Geophysical Journal International

Geophys. J. Int. (2010) **183,** 1443–1454 doi: 10.1111/j.1365-246X.2010.04794.x

First-order reflection/transmission coefficients for unconverted plane *P* waves in weakly anisotropic media

Véronique Farra[1] and Ivan Pšenčík[2]

[1] *Institut de Physique du Globe de Paris, 4 Place Jussieu, 75252 Paris Cedex 05, France*
[2] *Institute of Geophysics, Academy of Sciences of Czech Republic, Boční II,* 141 31 *Praha* 4, *Czech Republic. E-mail: ip@ig.cas.cz*

Accepted 2010 August 27. Received 2010 August 27; in original form 2010 March 14

SUMMARY

We present approximate formulae for the plane-wave displacement reflection/transmission (R/T) coefficients for interfaces of arbitrary contrast, separating two homogeneous, weakly anisotropic media. They result from boundary conditions requiring continuity of displacement vector and traction, in which coupled S waves are considered as a single S wave and exact quantities are replaced by first-order quantities used in first-order ray tracing. Specifically, the phase velocities, slowness and polarization vectors of P and coupled S waves appearing in the boundary conditions are of the first-order with respect to the deviations of anisotropy from isotropy. Application of the derived R/T coefficients transforms the amplitude of an incident P wave into amplitudes of reflected/transmitted P or coupled S waves. Coefficients can be computed for any incidence angle between 0° and 90°, and for any azimuth. In this paper, we test the accuracy of the derived R/T coefficients of unconverted plane P waves. We show that, except for critical regions, first-order coefficients approximate the exact coefficients with accuracy comparable or better than accuracy of linearized weak-contrast coefficients, which are, however, applicable only in subcritical regions.

Key words: Body waves; Seismic anisotropy; Wave propagation.

1 INTRODUCTION

In our previous papers, we studied the first-order ray tracing and dynamic ray tracing (FORT and FODRT) of seismic body P and coupled S waves propagating in *smoothly varying*, weakly anisotropic media without interfaces (Pšenčík & Farra 2005, 2007; Farra & Pšenčík 2008, 2010). The FORT and FODRT equations in the earlier references were derived using the perturbation theory, in which deviations of anisotropy from isotropy were considered to be of the first order. In such media, S waves are coupled and propagate as one wave with frequency-dependent amplitudes computed along a common S-wave ray. We obtained the FORT and FODRT equations for P or coupled S waves by replacing exact P-wave eigenvalues or the average of exact S-wave eigenvalues of the Christoffel matrix by their first-order counterparts in the ray tracing and dynamic ray tracing equations. In this way, the resulting equations generate first-order rays (in case of S waves, common S-wave rays) with first-order traveltimes, first-order slowness vectors and first-order geometrical spreading along them.

In this paper, we concentrate on computing first-order reflection/transmission (R/T) coefficients with the goal to extend the applicability of the FORT and FODRT equations to inhomogeneous, weakly anisotropic media with structural interfaces. As in the exact problem of reflection/transmission, the incident and generated waves satisfy boundary conditions corresponding to the given configuration. In the case of two elastic, weakly anisotropic solids in welded contact, these conditions are continuity of displacement and traction. The quantities appearing in the boundary conditions are first-order phase velocities, slowness and polarization vectors, with which we work in the FORT and FODRT.

The study of the R/T problem in anisotropic media has a rather long history. The problem of reflection/transmission of plane waves at a planar interface between two homogeneous anisotropic half-spaces was studied, for example, by Fedorov (1968), Musgrave (1970), Daley & Hron (1977), Graebner (1992), Schoenberg & Protázio (1992) and Chapman (1994, 2004). For more references see Červený (2001). Gajewski & Pšenčík (1987) used the plane-wave R/T coefficients in the ray-theory computations of seismic wavefields in 3-D laterally varying layered anisotropic media. Considerable attention has been paid to various simplifications of R/T coefficients based, for example, on the assumption of a weak-contrast interface, with anisotropy of the surrounding media of arbitrary strength (e.g. Ursin & Haugen 1996; Klimeš 2003) or on the assumption of a weak-contrast interface and weak anisotropy of the surrounding media (e.g. Rueger 1997, 2002; Vavryčuk & Pšenčík 1998; Zillmer *et al.* 1998; Vavryčuk 1999; Jílek 2002).

In this paper, we make no weak-contrast interface assumption. We only assume that the media on both sides of the interface are weakly, but generally anisotropic. Because the coupled S wave is considered as a single wave, the formulation of the reflection/transmission problem in this paper resembles closely the formulation for isotropic media. Although the derived formulae hold

for any type of incident wave, in numerical tests we concentrate on incident P waves only. An incident P wave can generate two possible types of waves, P or coupled S waves. The slowness vectors of generated waves are sought by solving numerically the corresponding first-order eikonal equation, separately for each generated wave. The corresponding R/T coefficient is determined by solving a system of six inhomogeneous, linear, algebraic equations. For media with anisotropy of higher symmetry, with specific orientation of symmetry elements with respect to the interface, it might be possible to find weak-anisotropy approximations of explicit exact expressions for the R/T coefficients derived by, for example Daley & Hron (1977) and Graebner (1992). Here, however, we consider the case of general anisotropy.

The main reason for this study is to test accuracy of approximate R/T coefficients, which we are going to use in the FORT and FODRT modelling in laterally varying, layered, weakly anisotropic media. Because their use eliminates problems of exact R/T coefficients, in which incident or generated S waves propagate in singular directions or close to them, and because of the simpler structure of coefficients and easier way of their evaluation, the approximate R/T coefficients may find applications even outside FORT and FODRT. The cost of evaluation of approximate R/T coefficients is slightly higher than the cost of computation of exact R/T coefficients in isotropic media, but the reduction of the cost is not our goal here. In isotropic media, the approximate coefficients reduce to exact R/T coefficients.

In Section 2, we present first-order formulae for the displacement vector **u** and traction **T** of a P or a coupled S wave. Besides first-order slowness vectors, special attention is paid to the first-order formulae specifying the polarization vector (P waves) or the polarization plane (coupled S waves). These formulae are then used in the boundary conditions in Section 3. In Section 3.1, the formulae for and procedure of determining the first-order slowness vectors of generated waves are described. In Section 3.2, the set of six inhomogeneous linear algebraic equations, from which the first-order R/T coefficients can be determined (Section 4) is specified. In Section 5, the accuracy of the derived formulae for the case of unconverted P waves is studied. Together with the reflection and transmission coefficients, R_{PP} and T_{PP}, the accuracy of the first-order slowness and polarization vectors of generated waves is tested. To make the tests as simple and transparent as possible, two models of an isotropic half-space over a half-space of transversely isotropic medium with horizontal axis of symmetry (HTI) are considered. The main results are summarized in Section 6.

The lower-case indices i, j, k, l, ... take the values of 1,2,3, the upper-case indices I, J, K, L, ... take the values of 1,2. The Einstein summation convention over repeated indices is used. The upper index $[\mathcal{M}]$ is used to denote quantities related to the coupled S wave. To distinguish quantities related to reflected and transmitted waves, we use superscripts R and T, respectively. Quantities related to the incident wave have no superscript. Sometimes, when we discuss properties of all generated waves, we use the superscript G.

2 BASIC FORMULAE

The boundary conditions, which must be satisfied at an interface, involve displacement vectors **u** and tractions **T** of the incident and generated waves. They are formally the same as in the exact case (Section 2.1). Basic role in both of them is played by the vectorial amplitude factors. In Section 2.2, we present their first-order approximations with respect to deviations between anisotropy and isotropy for both P and coupled S waves. They are based on formulae derived by Pšenčík & Farra (2005, 2007) and Farra & Pšenčík (2008, 2010).

2.1 First-order displacement vector and traction

The first-order approximation of the displacement vector **u** of an incident or generated harmonic plane wave can be expressed as

$$\mathbf{u}(\mathbf{x},t) = \mathbf{U}\exp[-\mathrm{i}\omega(t-\mathbf{p}\cdot\mathbf{x})]\,. \tag{1}$$

Here i is the imaginary unit, ω is the circular frequency, **p** is the first-order slowness vector and **U** is the first-order vectorial amplitude factor.

The first-order slowness vector can be expressed as $\mathbf{p} = \mathbf{n}/c(\mathbf{n})$. Here **n** is a unit vector perpendicular to the wave front of the relevant wave and $c = c(\mathbf{n})$ is its first-order phase velocity. It can be determined from the corresponding first-order eigenvalues of the Christoffel matrix.

The components of traction **T** acting at an interface with unit normal **N** are given by the expression

$$T_i(\mathbf{x},t) = \tau_{ij}(\mathbf{x},t)N_j = \rho(\mathbf{x})a_{ijkl}(\mathbf{x})N_j u_{k,l}(\mathbf{x},t)\,. \tag{2}$$

See, for example, Gajewski & Pšenčík (1987) and Červený (2001). Here, τ_{ij} are components of the stress tensor, ρ denotes the density, a_{ijkl} the density-normalized elastic moduli and $u_{k,l} = \partial u_k/\partial x_l$. Inserting the expression (1) for the displacement vector into eq. (2) leads to

$$T_i = \mathrm{i}\omega\rho a_{ijkl}N_j U_k p_l \exp[-\mathrm{i}\omega(t-\mathbf{p}\cdot\mathbf{x})]\,. \tag{3}$$

The symbols U_k and p_k in eq. (3) are components of the first-order vectorial amplitude factor **U** and of the first-order slowness vector **p**, respectively.

2.2 First-order vectorial amplitude factor U

The first-order vectorial amplitude factor **U** of a plane P wave propagating in a homogeneous, weakly anisotropic medium can be expressed in the following way:

$$\mathbf{U} = \mathcal{C}\mathbf{f}^{[3]}\big(\mathbf{p}^{[3]}\big)\,. \tag{4}$$

S waves in weakly anisotropic media propagate coupled. Therefore, we deal with them here as with a single wave, which we call the common S wave. The first-order vectorial amplitude factor **U** of the common S wave propagating in a homogeneous weakly anisotropic medium can be written as:

$$\mathbf{U} = \mathcal{A}\mathbf{f}^{[1]}\big(\mathbf{p}^{[\mathcal{M}]}\big) + \mathcal{B}\mathbf{f}^{[2]}\big(\mathbf{p}^{[\mathcal{M}]}\big)\,. \tag{5}$$

The term $\mathcal{C}$ in (4) is the first-order scalar P-wave amplitude factor, the terms $\mathcal{A}$ and $\mathcal{B}$ in (5) are the first-order scalar S-wave amplitude factors. The vectors $\mathbf{f}^{[i]}$ in (4) and (5) are defined in the following way:

$$\mathbf{f}^{[3]}(\mathbf{p}) = \frac{(c(\mathbf{n}))^2}{V_P^2 - V_S^2}\big[B_{13}(\mathbf{p})\mathbf{e}^{[1]}(\mathbf{p}) + B_{23}(\mathbf{p})\mathbf{e}^{[2]}(\mathbf{p})\big] + \mathbf{e}^{[3]}(\mathbf{p}) \tag{6}$$

and

$$\mathbf{f}^{[K]}(\mathbf{p}) = \mathbf{e}^{[K]}(\mathbf{p}) - \frac{(c(\mathbf{n}))^2}{V_P^2 - V_S^2}B_{K3}(\mathbf{p})\mathbf{e}^{[3]}(\mathbf{p})\,. \tag{7}$$

The vector $\mathbf{f}^{[3]}$ ($\mathbf{p}^{[3]}$) in eq. (4) is the first-order P-wave polarization vector. It is obtained from eq. (6) by specifying $c = c^{[3]}$ and $\mathbf{p} = \mathbf{p}^{[3]} = \mathbf{n}/c^{[3]}$, where $c^{[3]}$ and $\mathbf{p}^{[3]}$ are the first-order P-wave phase velocity

and slowness vector, respectively. Eq. (6) follows from eq. (14) of Pšenčík & Farra (2007). Vectors $\mathbf{f}^{[K]} = \mathbf{f}^{[K]}(\mathbf{p}^{[\mathcal{M}]})$ in eq. (5) are two vectors, to which amplitude factors $\mathcal{A}$ and $\mathcal{B}$ are related. Vectors $\mathbf{f}^{[K]}(\mathbf{p}^{[\mathcal{M}]})$ are obtained from eq. (7) by specifying $c = c^{[\mathcal{M}]}$ and $\mathbf{p} = \mathbf{p}^{[\mathcal{M}]} = \mathbf{n}/c^{[\mathcal{M}]}$, where $c^{[\mathcal{M}]}$ and $\mathbf{p}^{[\mathcal{M}]}$ are the first-order common S-wave phase velocity and slowness vector, respectively. The first-order S-wave polarization plane defined by vectors $\mathbf{f}^{[K]}(\mathbf{p}^{[\mathcal{M}]})$ is perpendicular to vector $\mathbf{f}^{[3]} = \mathbf{f}^{[3]}(\mathbf{p}^{[\mathcal{M}]})$. By using $\mathbf{p}^{[\mathcal{M}]}$ as an argument in $\mathbf{f}^{[3]}(\mathbf{p}^{[\mathcal{M}]})$, we emphasize that $\mathbf{f}^{[3]}(\mathbf{p}^{[\mathcal{M}]})$ is a vector related to the common S-wave ray and it differs from $\mathbf{f}^{[3]}$ $(\mathbf{p}^{[3]})$ (see eq. 4) related to the P-wave ray. Eq. (7) follows from eq. (13) of Farra & Pšenčík (2010).

Symbols B_{13} and B_{23} in eqs (6) and (7) are elements of symmetric matrix $\mathbf{B}$ $(\mathbf{p})$ ($\mathbf{p} = \mathbf{p}^{[3]}$ for P waves and $\mathbf{p} = \mathbf{p}^{[\mathcal{M}]}$ for coupled S waves) with elements:

$$B_{jl}(\mathbf{p}) = \Gamma_{ik}(\mathbf{p}) e_i^{[j]} e_k^{[l]} \,. \tag{8}$$

Terms $\Gamma_{ik}(\mathbf{p})$ are elements of the generalized Christoffel matrix $\mathbf{\Gamma}$ $(\mathbf{p})$:

$$\Gamma_{ik}(\mathbf{p}) = a_{ijkl} p_j p_l \,, \tag{9}$$

where a_{ijkl} are density-normalized elastic moduli. Symbols $e_i^{[j]}$ in eqs (6), (7) and (8) denote the components of three mutually perpendicular unit vectors $\mathbf{e}^{[j]}$. Vector $\mathbf{e}^{[3]}$ has been chosen so that $\mathbf{e}^{[3]} = \mathbf{n}$. Here $\mathbf{n}$ is a unit vector perpendicular to the wave front, specifying the direction of the first-order slowness vector $\mathbf{p}$ (with components p_i) of the corresponding wave. The remaining two mutually perpendicular unit vectors $\mathbf{e}^{[1]}$ and $\mathbf{e}^{[2]}$ can be chosen arbitrarily in the plane perpendicular to vector $\mathbf{e}^{[3]} = \mathbf{n}$. Vector $\mathbf{e}^{[3]}$ related to a P wave represents the zero-order approximation of the polarization vector, vector $\mathbf{f}^{[3]}$ $(\mathbf{p}^{[3]})$ represents its first-order approximation. Vectors $\mathbf{e}^{[K]}$ related to a common S wave specify the zero-order approximation of the S-wave polarization plane, vectors $\mathbf{f}^{[K]}(\mathbf{p}^{[\mathcal{M}]})$ specify its first-order approximation. Because vectors $\mathbf{e}^{[j]}$ are unit, eqs (6) and (7) imply that vectors $\mathbf{f}^{[i]}$ are generally non-unit and are different for P waves when they depend on $c^{[3]}$ and $\mathbf{p}^{[3]}$ and for common S waves when they depend on $c^{[\mathcal{M}]}$ and $\mathbf{p}^{[\mathcal{M}]}$.

Slowness vector $\mathbf{p}$ must satisfy the corresponding first-order eikonal equation

$$G(\mathbf{p}) = 1 \,. \tag{10}$$

Symbol G represents either the first-order approximation of the eigenvalue $G^{[3]}$ of the Christoffel matrix (9), corresponding to the P wave, or an average of the first-order eigenvalues $G^{[1]}$ and $G^{[2]}$ of the Christoffel matrix (9), corresponding to S waves. The explicit form of the first-order eikonal equations for P and coupled S waves can be found in Pšenčík & Farra (2005) and Farra & Pšenčík (2008). The first-order eigenvalues $G^{[m]}$ are closely related to the phase velocities of the corresponding waves

$$\left(c^{[\mathcal{M}]}(\mathbf{n})\right)^2 = \frac{1}{2}\left[G^{[1]}(\mathbf{n}) + G^{[2]}(\mathbf{n})\right], \quad \left(c^{[3]}(\mathbf{n})\right)^2 = G^{[3]}(\mathbf{n}) \,. \tag{11}$$

Symbols V_P and V_S in eqs (6) and (7) denote the P- and S-wave velocities corresponding to the reference isotropic medium closely approximating the studied weakly anisotropic medium at the point of incidence. Farra & Pšenčík (2010) showed that, for coupled S waves, the reference velocities must be chosen in the following way:

$$V_S^2 = \left(c^{[\mathcal{M}]}\right)^2, \quad V_P^2 = \left(c^{[\mathcal{M}]}\right)^2 B_{33}\left(\mathbf{p}^{[\mathcal{M}]}\right) . \tag{12}$$

We can proceed similarly for P waves and choose:

$$V_P^2 = \left(c^{[3]}\right)^2, \quad V_S^2 = \frac{1}{2}\left(c^{[3]}\right)^2\left[B_{11}\left(\mathbf{p}^{[3]}\right) + B_{22}\left(\mathbf{p}^{[3]}\right)\right] . \tag{13}$$

We can then modify eq. (6) to read

$$\mathbf{f}^{[3]}\left(\mathbf{p}^{[3]}\right) = \frac{B_{13}\left(\mathbf{p}^{[3]}\right)\mathbf{e}^{[1]}\left(\mathbf{p}^{[3]}\right) + B_{23}\left(\mathbf{p}^{[3]}\right)\mathbf{e}^{[2]}\left(\mathbf{p}^{[3]}\right)}{1 - \frac{1}{2}\left[B_{11}\left(\mathbf{p}^{[3]}\right) + B_{22}\left(\mathbf{p}^{[3]}\right)\right]} + \mathbf{e}^{[3]}\left(\mathbf{p}^{[3]}\right) \tag{14}$$

and eq. (7) to read

$$\mathbf{f}^{[K]}\left(\mathbf{p}^{[\mathcal{M}]}\right) = \mathbf{e}^{[K]}\left(\mathbf{p}^{[\mathcal{M}]}\right) + \frac{B_{K3}\left(\mathbf{p}^{[\mathcal{M}]}\right)}{1 - B_{33}\left(\mathbf{p}^{[\mathcal{M}]}\right)}\mathbf{e}^{[3]}\left(\mathbf{p}^{[\mathcal{M}]}\right) . \tag{15}$$

3 BOUNDARY CONDITIONS

Let us consider two homogeneous weakly anisotropic half-spaces in welded contact, separated by planar interface Σ with unit normal $\mathbf{N}$ pointing into the medium in which the incident plane wave propagates. The medium in which the incident wave propagates is specified by density $\rho^{(1)}$ and the density-normalized elastic moduli $a_{ijkl}^{(1)}$. The medium on the other side of the interface is specified by $\rho^{(2)}$ and $a_{ijkl}^{(2)}$. An incident wave generates reflected P and coupled S waves in the half-space specified by $\rho^{(1)}$ and $a_{ijkl}^{(1)}$, and transmitted P and coupled S waves in the half-space specified by $\rho^{(2)}$ and $a_{ijkl}^{(2)}$. The incident and generated waves satisfy the boundary conditions, which in the case of an interface separating two solid media, consist of the requirements of continuity of displacement $\mathbf{u}$ and traction $\mathbf{T}$ across the interface.

The boundary conditions lead to two sets of equations. The first set, resulting from the continuity of the traveltime of all involved waves across the interface, represents equations for determining the slowness vectors of generated waves. The second set, resulting from the boundary conditions themselves, represents equations for determining the scalar amplitude factors of generated waves. In the following, we deal successively with both sets of equations.

3.1 Transformation of slowness vectors across an interface

The continuity of traveltime along the interface Σ implies the continuity of the traveltime derivatives taken along the interface. This can be expressed in the following way:

$$\mathbf{p}^G - (\mathbf{p}^G \cdot \mathbf{N})\mathbf{N} = \mathbf{p} - (\mathbf{p} \cdot \mathbf{N})\mathbf{N} \,. \tag{16}$$

Here, $\mathbf{p}$ and $\mathbf{p}^G$ are first-order slowness vectors of the incident and generated (G) waves, $\mathbf{N}$ is the unit normal to interface Σ. Eq. (16) represents Snell's Law for anisotropic media. From eq. (16) we can determine the components of the slowness vectors of the generated waves, tangential to the interface. It remains to determine their components along the normal $\mathbf{N}$ to the interface. We can express the slowness vector of any generated wave as

$$\mathbf{p}^G = \mathbf{b} + \xi^G \mathbf{N} = \mathbf{p} - (\mathbf{p} \cdot \mathbf{N})\mathbf{N} + \xi^G \mathbf{N} \,. \tag{17}$$

In eq. (17), ξ^G represents the scalar component of $\mathbf{p}^G$ parallel to $\mathbf{N}$, and $\mathbf{b}$ represents the vectorial component of $\mathbf{p}^G$, tangential to Σ. Components ξ^G of all generated waves are the sought parameters. They can be found from the first-order eikonal equations satisfied by the waves generated on corresponding sides of the interface

$$G(\mathbf{b} + \xi^G \mathbf{N}) = 1 \,. \tag{18}$$

Eikonal equation (18) can be rewritten into the form of a polynomial equation of the fourth degree in ξ^G. It has four roots, two of which are non-physical. They can be identified as two conjugate roots, whose imaginary parts are larger than the imaginary parts of the remaining two roots. Of the remaining two roots, we accept the one which

belongs to the wave whose first-order ray-velocity vector $\mathbf{v}^G(v_i^G = \frac{1}{2}\partial G/\partial p_i$, where $G = G^{[3]}$ for P waves, or $G = \frac{1}{2}(G^{[1]} + G^{[2]})$ for coupled S waves) points into the medium in which the generated wave should propagate (in the case of real roots), or which satisfies the radiation condition (in the case of complex conjugate roots). Explicitly this means that $N_i v_i^G > 0$ for reflected and $N_i v_i^G < 0$ for transmitted waves in the case of real roots, and Im $\xi^G > 0$ for reflected and Im $\xi^G < 0$ for transmitted waves in the case of complex conjugate roots. The waves corresponding to the real roots of the polynomial equation are regular waves while those related to the complex roots are evanescent waves.

The selection of roots described earlier is necessary when we use a polynomial equation solver, which provides all four roots. We can, however, also use alternative procedures in which we seek just the relevant root, and the selection of roots is not necessary. In weakly anisotropic media, it is reasonable to assume that the sought root of eq. (18) is close to the root $\xi^{G(0)}$ of a similar equation corresponding to a reference isotropic medium. We can thus use the root from the reference isotropic case as an initial guess of the sought root. Jech & Pšenčík (1989, Section 4.3) proposed a one-step procedure based on the first-order correction of such an initial guess $\xi^{G(0)}$. Recently, Vanelle & Gajewski (2009) made the procedure iterative, successively updating the reference isotropic medium. The procedure proposed and used by Dehghan *et al.* (2007) seems to be more efficient. They also use $\xi^{G(0)}$, determined for a reference isotropic medium, as the initial value in the iterative search for the solution of eq. (18). Rather than updating the reference medium, they use the Newton–Raphson iterative method to update the root itself. The iterative formula, derived from the expansion of the eigenvalue G in eq. (18) with respect to ξ^G, reads

$$\mathbf{p}^{G\{j\}} = \mathbf{b} + \xi^{G\{j\}}\mathbf{N}\,, \tag{19}$$

where j is the iteration number and

$$\xi^{G\{j\}} = \xi^{G\{j-1\}} - \frac{G\left(\mathbf{p}^{G\{j-1\}}\right) - 1}{N_k \partial G/\partial p_k\left(\mathbf{p}^{G\{j-1\}}\right)}\,. \tag{20}$$

The explicit expressions for G and $\partial G/\partial p_k$ for P waves in media of arbitrary anisotropy and for coupled S waves in media of orthorhombic and TI symmetries can be found in Pšenčík & Farra (2007) and Farra & Pšenčík (2008), respectively. The expression for $\partial G/\partial p_k$ for coupled S waves in media of arbitrary anisotropy can be simply determined by differentiating eq. (19) of Farra & Pšenčík (2008) with respect to p_k.

The use of eqs (19) and (20) avoids the necessity of seeking the best-fitting reference medium (Vanelle & Gajewski 2009). The procedure described earlier can be used even for stronger anisotropy (within weak-anisotropy approximation) and arbitrary incidence angles, including large ones as shown in the examples in Section 5. It can also be used to seek the roots of eq. (18) for evanescent waves, that is to seek complex-valued roots.

3.2 Transformation of amplitudes across an interface

Let us now apply the continuity conditions of the displacement vector (1) and the traction (3) to the system of incident, reflected and transmitted waves. The continuity of traveltime along interface Σ leads to the equality of the exponential factors of displacement vectors of incident and generated waves. Taking this into account, we can express the boundary conditions as follows:

$$\begin{aligned}
&\mathcal{A}^R f_i^{[1]R} + \mathcal{B}^R f_i^{[2]R} + \mathcal{C}^R f_i^{[3]R} - \mathcal{A}^T f_i^{[1]T} - \mathcal{B}^T f_i^{[2]T} - \mathcal{C}^T f_i^{[3]T} = -U_i,\\
&\mathcal{A}^R X_i^{[1]R} + \mathcal{B}^R X_i^{[2]R} + \mathcal{C}^R X_i^{[3]R} - \mathcal{A}^T X_i^{[1]T} - \mathcal{B}^T X_i^{[2]T} - \mathcal{C}^T X_i^{[3]T} = -X_i,
\end{aligned} \tag{21}$$

where

$$\begin{aligned}
X_i &= \rho^{(1)} a_{ijkl}^{(1)} N_j U_k p_l,\\
X_i^{[3]R} &= \rho^{(1)} a_{ijkl}^{(1)} N_j f_k^{[3]R} p_l^{[3]R}, \quad X_i^{[3]T} = \rho^{(2)} a_{ijkl}^{(2)} N_j f_k^{[3]T} p_l^{[3]T},\\
X_i^{[N]R} &= \rho^{(1)} a_{ijkl}^{(1)} N_j f_k^{[N]R} p_l^{[\mathcal{M}]R}, \quad X_i^{[N]T} = \rho^{(2)} a_{ijkl}^{(2)} N_j f_k^{[N]T} p_l^{[\mathcal{M}]T}\,.
\end{aligned} \tag{22}$$

The symbols X_i in eqs (21) and (22) correspond to the incident wave, symbols $X_i^{[3]G}$ to generated P waves and $X_i^{[N]G}$, $N = 1, 2$, to generated coupled S waves (the superscript G stands for R, reflected, or T, transmitted). The slowness vectors of generated waves are determined by the procedure described in the preceding section. Vectors $\mathbf{f}^{[i]G}$ can be determined from eqs (6) or (7) or, alternatively, from eqs (14) or (15).

4 *R*/*T* COEFFICIENTS FOR AN INCIDENT *P* WAVE

For an incident P wave, the quantities U_i and X_i on the right-hand side of eq. (21) follow from (4) and from the first equation in eq. (22), in which U_k again follows from (4) and p_l are the components of the P-wave first-order slowness vector $\mathbf{p}^{[3]}$.

Eq. (21) represents a set of six inhomogeneous linear algebraic equations for six unknowns $\mathcal{A}^R$, $\mathcal{B}^R$, $\mathcal{C}^R$, $\mathcal{A}^T$, $\mathcal{B}^T$ and $\mathcal{C}^T$, the first-order scalar amplitude factors of four waves generated by incidence of the wave with the first-order vectorial amplitude factor $\mathbf{U}$. If we wish to compute the standard displacement R/T coefficients, we have to modify eqs (21) and (22). It is necessary to normalize the vectors $\mathbf{f}^{[3]}$ and $\mathbf{f}^{[i]G}$ in eqs (21) and (22) to unit vectors, and to replace them by their normalized counterparts $\bar{\mathbf{f}}^{[3]}$ and $\bar{\mathbf{f}}^{[i]G}$. Normalized vectors $\bar{\mathbf{f}}^{[I]G}(\mathbf{p}^{[\mathcal{M}]})$ can be chosen arbitrarily in the plane perpendicular to vector $\mathbf{f}^{[3]G}(\mathbf{p}^{[\mathcal{M}]})$. First-order R/T coefficients can be then introduced as $R_{PP} = \nu^{[3]R}\mathcal{C}^R/\mathcal{C}$, $T_{PP} = \nu^{[3]T}\mathcal{C}^T/\mathcal{C}$, $R_{PS[1]} = \nu^{[1]R}\mathcal{A}^R/\mathcal{C}$, $R_{PS[2]} = \nu^{[2]R}\mathcal{B}^R/\mathcal{C}$, $T_{PS[1]} = \nu^{[1]T}\mathcal{A}^T/\mathcal{C}$ and $T_{PS[2]} = \nu^{[2]T}\mathcal{B}^T/\mathcal{C}$, where $\nu^{[i]R} = |\mathbf{f}^{[i]R}|/|\mathbf{f}^{[3]}|$ and $\nu^{[i]T} = |\mathbf{f}^{[i]T}|/|\mathbf{f}^{[3]}|$. Indices $S[1]$ and $S[2]$ indicate that the corresponding coefficients are related to vectors $\bar{\mathbf{f}}^{[1]G}$ or $\bar{\mathbf{f}}^{[2]G}$, respectively. Eqs (21) and (22) can now be rewritten in the following form:

$$\begin{aligned}
&R_{PS[1]}\bar{f}_i^{[1]R} + R_{PS[2]}\bar{f}_i^{[2]R} + R_{PP}\bar{f}_i^{[3]R} - T_{PS[1]}\bar{f}_i^{[1]T}\\
&\quad - T_{PS[2]}\bar{f}_i^{[2]T} - T_{PP}\bar{f}_i^{[3]T} = -\bar{f}_i^{[3]},\\
&R_{PS[1]}\bar{X}_i^{[1]R} + R_{PS[2]}\bar{X}_i^{[2]R} + R_{PP}\bar{X}_i^{[3]R} - T_{PS[1]}\bar{X}_i^{[1]T}\\
&\quad - T_{PS[2]}\bar{X}_i^{[2]T} - T_{PP}\bar{X}_i^{[3]T} = -\rho^{(1)} a_{ijkl}^{(1)} N_j \bar{f}_k^{[3]} p_l\,,
\end{aligned} \tag{23}$$

where

$$\begin{aligned}
\bar{X}_i^{[3]R} &= \rho^{(1)} a_{ijkl}^{(1)} N_j \bar{f}_k^{[3]R} p_l^{[3]R}\,, \quad \bar{X}_i^{[3]T} = \rho^{(2)} a_{ijkl}^{(2)} N_j \bar{f}_k^{[3]T} p_l^{[3]T},\\
\bar{X}_i^{[N]R} &= \rho^{(1)} a_{ijkl}^{(1)} N_j \bar{f}_k^{[N]R} p_l^{[\mathcal{M}]R}, \quad \bar{X}_i^{[N]T} = \rho^{(2)} a_{ijkl}^{(2)} N_j \bar{f}_k^{[N]T} p_l^{[\mathcal{M}]T}\,.
\end{aligned} \tag{24}$$

5 EXAMPLES

In this section, the system of eqs (23) with (24) is solved numerically to evaluate the first-order R_{PP} and T_{PP} coefficients. Because we are interested in unconverted P waves, the choice of vectors $\bar{\mathbf{f}}^{[I]}(\mathbf{p}^{[\mathcal{M}]})$ in

the plane perpendicular to $\mathbf{f}^{[3]}(\mathbf{p}^{[\mathcal{M}1]})$ can be arbitrary. We determine them from eq. (15), in which vector $\mathbf{e}^{[2]}$ is chosen to be horizontal and all three vectors $\mathbf{e}^{[i]}$ form an orthonormal right-handed vectorial basis.

For tests of accuracy of the first-order coefficients and related quantities, we use the two models used by Pšenčík & Vavryčuk (1998). In both models, we consider an isotropic upper half-space, in which incident and reflected waves propagate, and the lower half-space with transversely isotropic medium with horizontal axis of symmetry (HTI), in which transmitted waves propagate. The HTI half-space is the same in both models. The models differ only in the isotropic upper half-space. In the first model, Model A, the *P*- and *S*-wave velocities and density of the upper half-space are $\alpha = 4.0\ \mathrm{km\,s^{-1}}$, $\beta = 2.31\ \mathrm{km\,s^{-1}}$ and $\rho = 2.65\ \mathrm{g\,cm^{-3}}$, respectively. In the second model, Model B, these parameters are $\alpha = 3.0\ \mathrm{km\,s^{-1}}$, $\beta = 1.73\ \mathrm{km\,s^{-1}}$ and $\rho = 2.2\ \mathrm{g\,cm^{-3}}$. The matrix of density-normalized elastic moduli (in $\mathrm{km^2\,s^{-2}}$) specifying the HTI medium of the lower half-space reads

$$\begin{pmatrix} 9.43 & 3.14 & 3.14 & 0.00 & 0.00 & 0.00 \\ & 15.27 & 4.60 & 0.00 & 0.00 & 0.00 \\ & & 15.27 & 0.00 & 0.00 & 0.00 \\ & & & 5.33 & 0.00 & 0.00 \\ & & & & 4.25 & 0.00 \\ & & & & & 4.25 \end{pmatrix} . \tag{25}$$

The density of the HTI medium is $\rho = 2.6\ \mathrm{g\,cm^{-3}}$. We can see that the axis of symmetry is oriented along the *x*-axis of the Cartesian coordinate system. The vertical sections of the phase-velocity surfaces containing the horizontal axis of symmetry are shown in Fig. 1. The *P*-wave velocity section is shown in the bottom plot, the *S*-wave velocity sections are shown in the top plot.

We can see that in Model A, the *P*- and *S*-wave velocities in the upper (isotropic) half-space exceed the *P*- and *S*-wave velocities in the lower half-space. Except in the vertical plane perpendicular to the axis of symmetry, the velocity contrast (ratio of the absolute value of the difference of velocities on both sides of the interface and of their average) varies with direction. For *P* waves in the vertical plane containing the axis of symmetry, the velocity contrast increases from about 2 per cent for vertical direction (0°) to about 26 per cent for horizontal direction (90°). For the S1 wave (faster, with *SH*-wave polarization) in the same vertical plane, the contrast increases from about 0.05 per cent to about 11 per cent. For the S2 wave (slower), the contrast varies slightly around 11 per cent. In Model B, the *P*- and *S*-wave velocities in the upper half-space are lower than in the lower half-space. The contrast is generally higher than in Model A. Its variation in the vertical plane containing the axis of symmetry is opposite to that for Model A. For the *P* wave, the contrast decreases from about 26 per cent for vertical direction to about 2 per cent for horizontal direction. For the *S*1 wave, the contrast decreases from about 29 to 17 per cent. For the *S*2 wave, the contrast varies slightly around 17 per cent. As to the anisotropy of the HTI half-space, it is about 24 per cent for the *P* wave and around 11 per cent for the *S*1 wave.

Coefficients R_{PP} and T_{PP} obtained by solving the system of equations (23) may be complex valued. Therefore, we present them in terms of their moduli and phases:

$$R_{PP} = |R_{PP}| \exp(\mathrm{i}\varphi_R) , \qquad T_{PP} = |T_{PP}| \exp(\mathrm{i}\varphi_T) . \tag{26}$$

The presented figures have the forms of maps, in which the quantities are shown as functions of the angle of incidence θ (horizontal axis) and of azimuth Φ (vertical axis). Both angles are specified in degrees. Azimuth $\Phi = 0^\circ$ corresponds to the direction along the axis of symmetry, $\Phi = 90^\circ$ to the direction perpendicular to the axis of symmetry. The incidence angle $\theta = 0^\circ$ corresponds to normal incidence. The angles specify direction of the first-order slowness vector of incident wave.

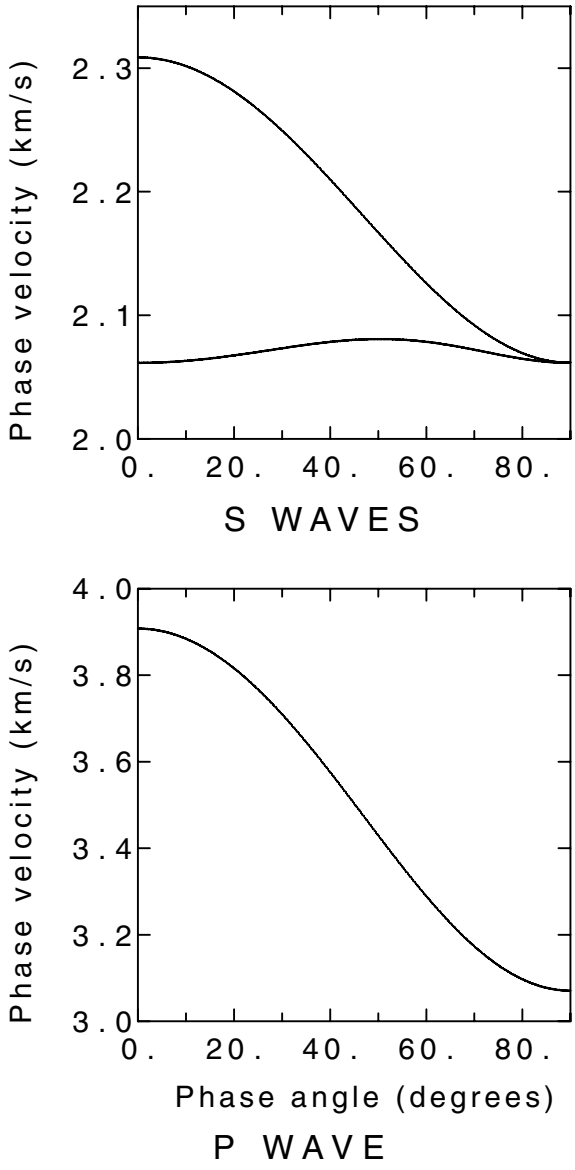

Figure 1. Variation of the *P*-wave (bottom) and *S*-wave (top) phase velocities in a vertical plane containing the axis of symmetry of the HTI medium specified in (25). The velocities vary from the vertical (0°) to horizontal (90°) direction of the wave normal.

For a better understanding of the behaviour of the approximate coefficients, we first show the maps of deviations of the first-order slowness vectors and of the first-order polarization vectors or the first-order polarization planes of waves generated in the lower anisotropic half-space from their exact counterparts. These deviations are expressed as angles (in degrees) between the approximate and exact vectors. We then show maps of the exact moduli and phases of the R_{PP} and T_{PP} coefficients (Fedorov 1968; Gajewski & Pšenčík 1987) followed by maps of differences of the moduli and phases of the first-order *R*/*T* coefficients from the exact ones.

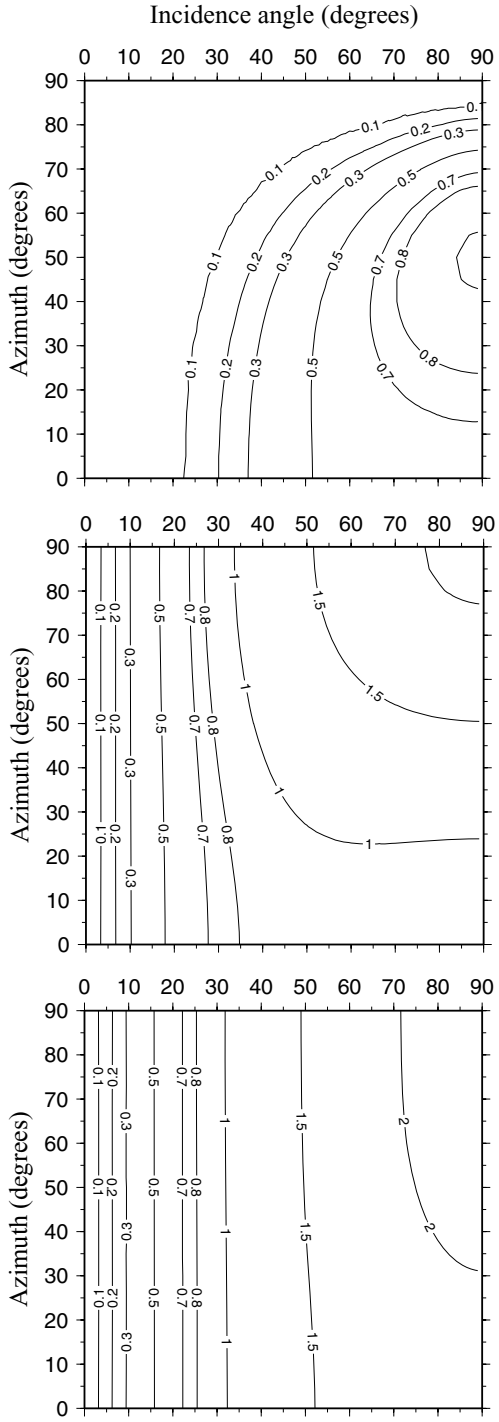

Figure 2. Maps of the angular deviations (in degrees) of the approximate from the exact slowness vectors of transmitted *P* (top), *S*1 (middle) and *S*2 (bottom) waves for Model A.

Fig. 2 shows the maps of angular deviations of the approximate from the exact slowness vectors of the transmitted *P* (top), *S*1 (middle) and *S*2 (bottom) waves for Model A. The *S*-wave plots show the deviations of the first-order slowness vectors of coupled *S* wave from the exact slowness vectors of *S*1 and *S*2 waves. Similar maps for the reflected *P* and *S* waves are not shown because the reflected waves propagate in the isotropic half-space, in which the approximate slowness vectors coincide with the exact vectors (thus their differences are zero for each incidence angle and azimuth).

We can see that the approximate slowness vectors of the *P* wave do not deviate from the exact vectors by more than 1°. The deviations increase with increasing angle of incidence, the maximum deviations occurring for azimuths around 50°. Deviations are zero and close to zero for azimuth 90° and azimuths close to it. The vertical plane with azimuth 90° is perpendicular to the axis of symmetry and thus coincides with the 'isotropy plane', in which directions of approximate slowness vectors coincide with exact slowness vectors. The situation is different in case of *S* waves (middle and bottom plots). The deviations also increase with increasing angle of incidence, being largest for azimuths around 90°. They are slightly larger than in the case of the *P* wave; they slightly exceed 2°. For azimuths close to 90°, we observe non-zero deviations. This is the consequence of studying the deviations of the first-order slowness vectors, corresponding to the coupled *S* wave, from the exact slowness vectors of separate *S*1 and *S*2 waves, as mentioned earlier.

We have also studied relative differences between the sizes of the approximate and exact slowness vectors. For *P* waves, the relative differences are lowest for incidence angles close to 0° or azimuths close to 90°. They are maximum (close to 1 per cent) along an approximately ellipsoidal curve connecting points with azimuth and incidence angle (0°, 53°) and (35°, 90°). For *S* waves, at the point with azimuth 0° and incidence angle 90°, the relative differences are 2.2 and −5.4 per cent for faster and slower *S* wave, respectively. From the above point, the relative differences increase radially to 5.2 per cent for faster *S* wave and decrease, also radially, to −6.2 per cent for slower *S* wave.

Fig. 3 shows the maps of angular deviations of the approximate from exact polarization of transmitted *P* (top) and *S* (bottom) waves for Model A. In the case of *P* waves, we show the deviation of the first-order polarization vector $\mathbf{f}^{[3]}$ ($\mathbf{p}^{[3]}$) obtained from eq. (6), from the exact one. In the case of *S* waves, we show the deviation of the normal to the first-order *S*-wave polarization plane, formed by vectors $\mathbf{f}^{[K]}(\mathbf{p}^{[\mathcal{M}]})$ obtained from eq. (7), from the normal to the exact *S*-wave polarization plane, defined by the exact *S*-wave polarization vectors. For the same reasons as in the case of the deviations of slowness vectors, the maps for reflected *P* and *S* waves are not shown. The behaviour of the polarization deviations is similar to the behaviour of the slowness vector deviations. In the case of *P* waves, the deviations of the polarization vectors are slightly larger, slightly exceeding 1.2°. The deviations for azimuths close to 90° are zero. The deviations of normals to the polarization planes of *S* waves resemble deviations of slowness vectors of *S* waves.

In Fig. 4, we can see maps of the modulus of the exact R_{PP} coefficient (top) and of the differences between the moduli of the first order and the exact R_{PP} coefficients (bottom) for Model A. Because of the higher velocities in the upper half-space, there is no critical incidence. For all the azimuths and incidence angles, the phases are 180° (therefore, we do not show the map of phases), which indicates that the coefficients are negative. The first-order coefficients also have phase 180°, therefore the differences in phase are zero everywhere and are not shown. Because the contrast is very weak for small angles of incidence, the modulus of the exact R_{PP} coefficient is rather small for small angles. As expected, modulus $|R_{PP}|$ increases, except for incidence angles close to 20° and azimuths between 0 and 40°, with increasing incidence angle. The slight decrease in $|R_{PP}|$ in the above-mentioned region is an effect observable only in anisotropic media. From the bottom plot, we can see that, for small incidence angles, the modulus of the approximate R_{PP} coefficient is less than the modulus of the exact one. Only for large azimuths and large incidence angles, is the modulus of the approximate coefficient slightly larger than the modulus of the exact

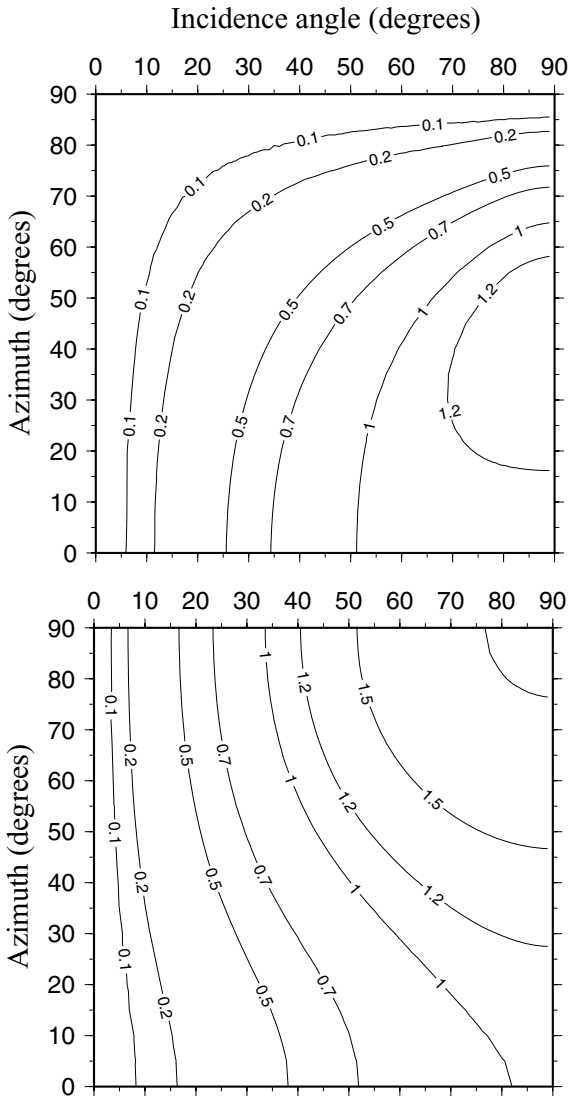

Figure 3. Map of the angular deviations (in degrees) of the approximate from the exact polarization vectors of transmitted *P* wave (top). Map of the angular deviations (in degrees) of the normal to the common *S*-wave polarization plane from the normal to the exact *S*-wave polarization plane (bottom). Both for Model A.

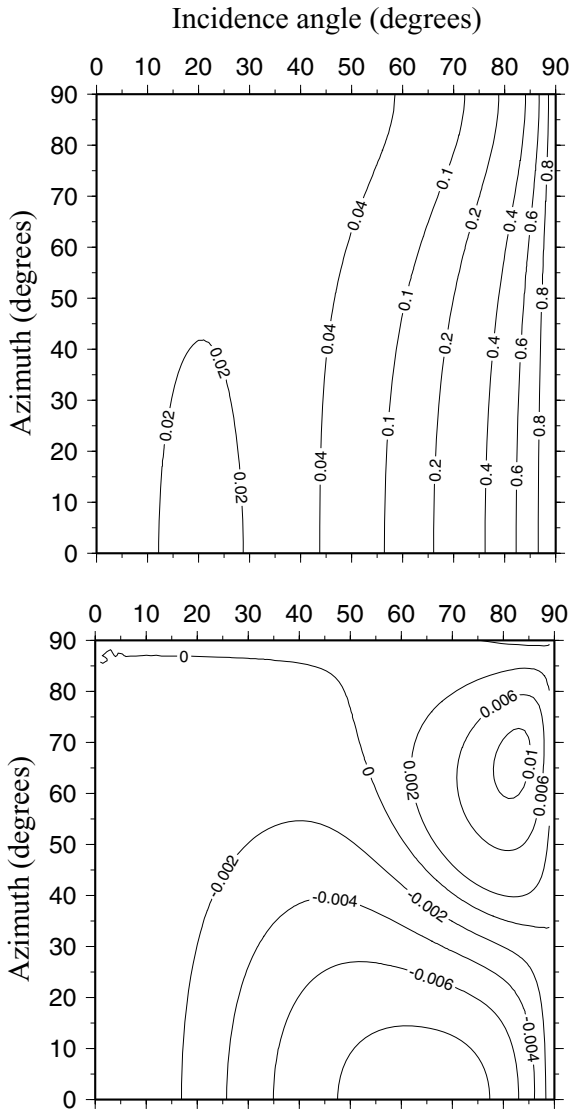

Figure 4. Maps of the moduli of the exact R_{PP} coefficient (top) and of the differences between the moduli of the first-order and exact R_{PP} coefficients (bottom) for Model A.

one. For azimuths close to 90° (the isotropy plane) or small angles of incidence, the approximate R_{PP} coefficient is very accurate. The deviation of the modulus of the approximate R_{PP} coefficient from the exact one is smaller by at least one order, but for most angles of incidence significantly less than exact modulus. The relative difference between moduli of the approximate and exact coefficients in regions in which the exact modulus of the coefficient is about 0.1 or larger does not exceed 3 per cent. In regions, where the exact modulus of the coefficient is very small, the relative errors are, of course, larger. They may reach 25 per cent.

Fig. 5 shows the same as Fig. 4, but for the transmission coefficient T_{PP} for Model A. The modulus of the T_{PP} coefficient decreases with increasing incidence angle. Due to the weak-contrast interface for small angles of incidence, the modulus of the T_{PP} coefficient is quite large for these angles. The phase is zero for any angle of incidence and azimuth. From the bottom plot, we can see that the modulus of the approximate T_{PP} coefficient is less than the exact one for all azimuths and angles of incidence. The differences are smaller than the values of the modulus by around two orders of magnitude. The maximum difference is about 0.015. The relative errors are less than 1 per cent for most angles, slightly exceeding 3 per cent for large incidence angles.

In the following figures, we show plots corresponding to Model B. As mentioned earlier, in this case the velocities in the isotropic upper half-space are smaller than in the anisotropic lower half-space. We can therefore observe critical and overcritical incidence of the *P* wave. The effects of critical and overcritical incidence can already be observed in maps of the angular deviations of approximate from exact slowness vectors.

Angular deviations of the first-order from exact slowness vectors of transmitted *P* (top), *S*1 (middle) and *S*2 (bottom) waves are shown in Fig. 6. If we compare the top plots of Figs 2 and 6, we can see a similar increase in deviations for increasing angles of incidence up to certain 'boundary' values (angles of incidence of about 75° for azimuths close to 0°, which continuously change to angles of incidence of about 50° for azimuths close to 90°). The deviations in the upper plot of Fig. 6 grow quickly around these 'boundary' values

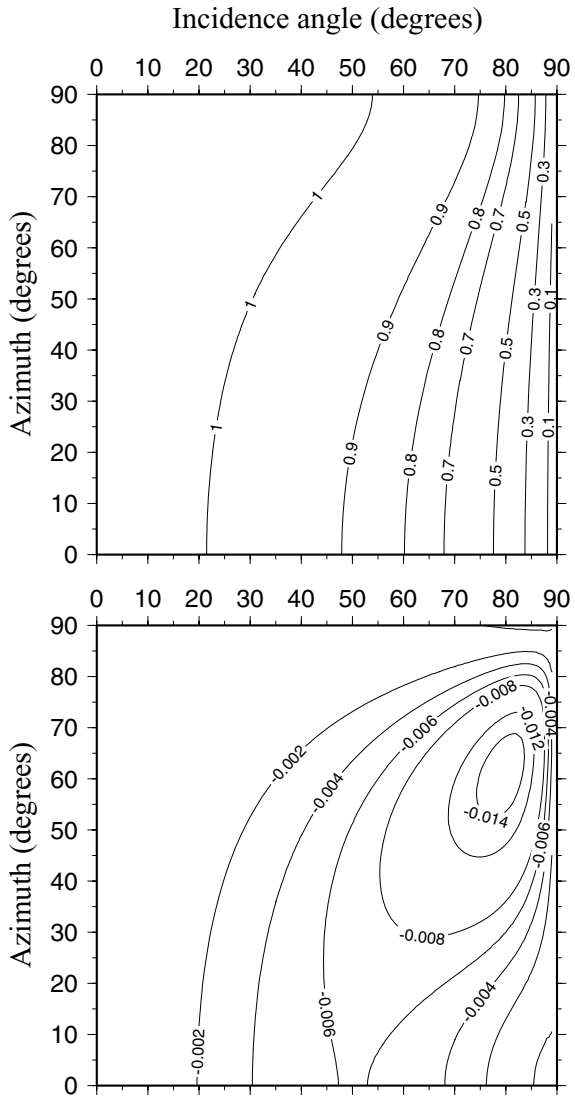

Figure 5. Maps of the moduli of the exact T_{PP} coefficient (top) and of the differences between the moduli of the first-order and exact T_{PP} coefficients (bottom) for Model A.

of the angles of incidence. These angles of incidence indicate critical incidence. Because the angular positions of exact and approximate critical angles slightly differ, we can observe a narrow belt (instead of a sharp curve), in which the angular deviations increase over the value of about 3°, the maximum value in the subcritical region. In the overcritical region, the differences are zero. This is because we are comparing the real parts of the complex-valued first-order and exact slowness vectors in this region. The real parts are in both cases tangent to the interface and have the same size. Thus their differences are zero. As in Fig. 2, the differences for the azimuths close to 90° are negligible. The slowness vectors of transmitted *S* waves are not affected by overcritical incidence and, therefore, the behaviour of their deviations is very similar to the behaviour of their counterparts in Model A, shown in the middle and bottom plots of Fig. 2. The deviations in Model B attain greater values (up to around 3°) as a consequence of the lower velocities in the upper half-space than in the lower.

The relative differences between the sizes of the approximate and exact slowness vectors have a similar character to those obtained in

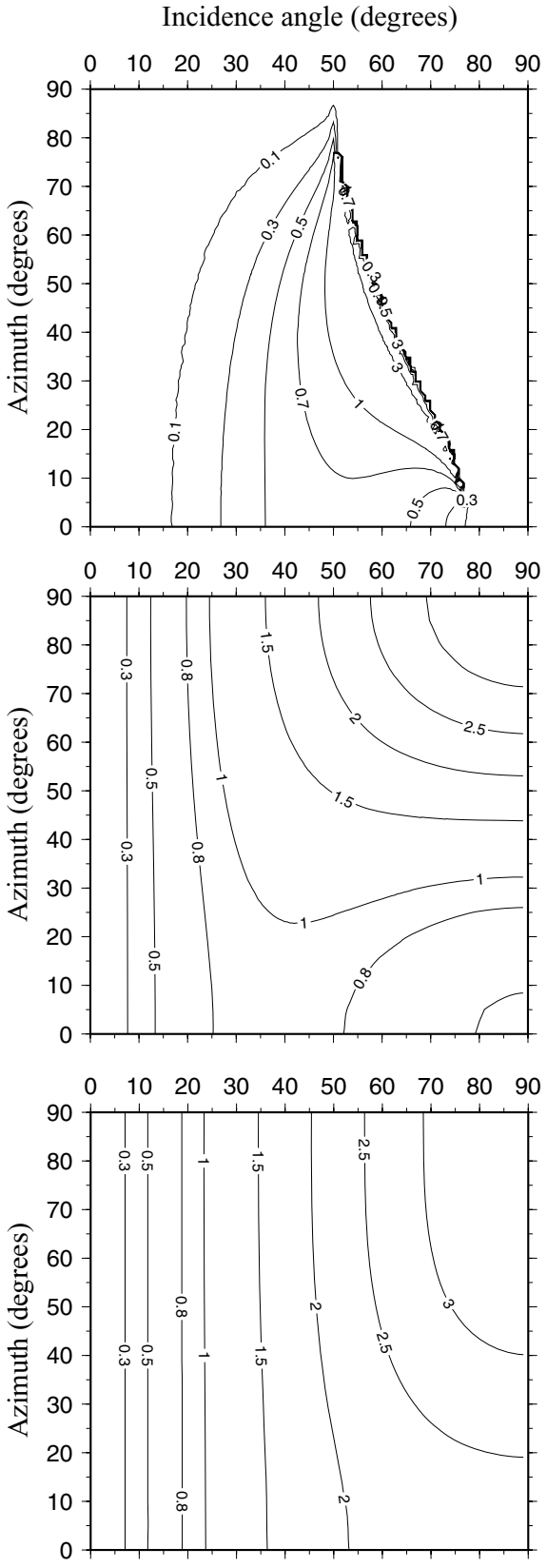

Figure 6. Maps of the angular deviations (in degrees) of the approximate from the exact slowness vectors of transmitted *P* (top), *S*1 (middle) and *S*2 (bottom) waves for Model B.

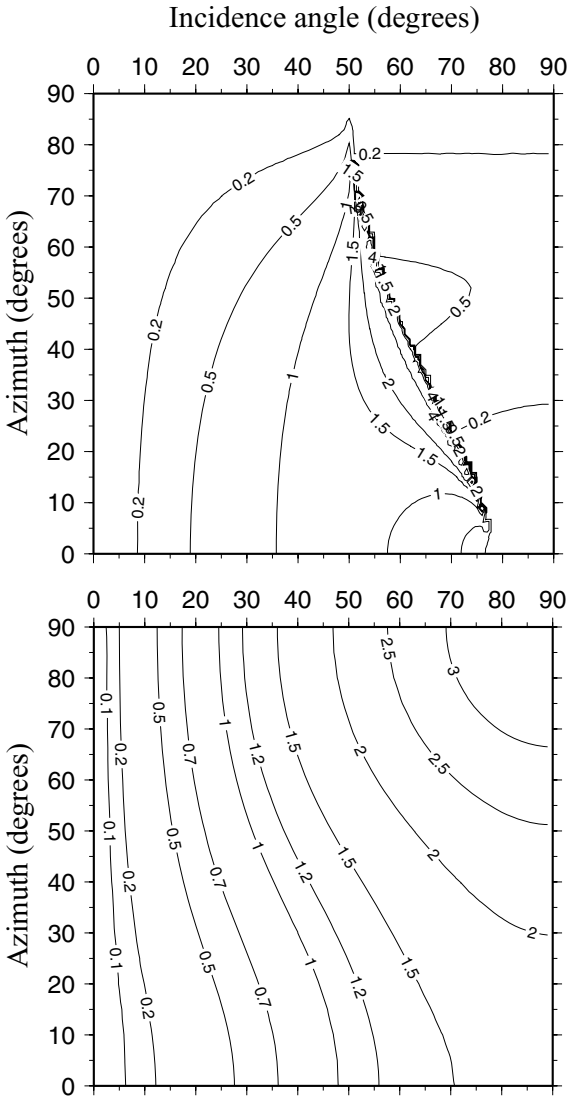

Figure 7. Map of the angular deviations (in degrees) of the approximate from the exact polarization vectors of transmitted *P* wave (top). Map of the angular deviations (in degrees) of the normal to the common *S*-wave polarization plane from the normal to the exact *S*-wave polarization plane (bottom). Both for Model B.

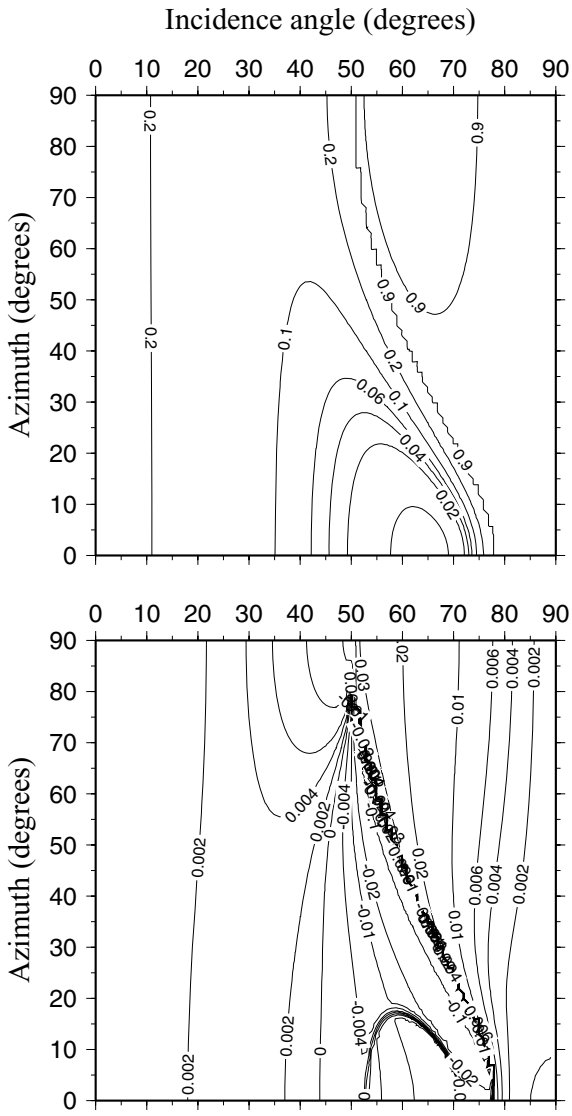

Figure 8. Maps of the moduli of the exact R_{PP} coefficient (top) and of the differences between the moduli of the first-order and exact R_{PP} coefficients (bottom) for Model B.

Model A. The only exception is behaviour of differences obtained for *P* waves. The differences exist only in the subcritical region (like in the upper plot of Fig. 6). They are zero in overcritical region due to reasons described in the previous paragraph.

In the upper plot of Fig. 7, which shows the angular deviations of the first-order from exact polarization vectors of the transmitted *P* wave (in the overcritical region we compare real parts of the complex-valued first-order and exact polarization vectors), we can again observe a narrow belt of strongly increased values of deviations, which indicates the region of critical incidence. In the subcritical region, the differences behave in a similar way as in the upper plot of Fig. 3, with slightly higher angular deviations of the first-order from exact polarization vectors, which are again the consequence of lower velocities in the upper half-space. This is also true for any angle of incidence and azimuth for the *S*-wave polarization differences shown in the bottom plot of Fig. 7; compare this plot and the bottom plot of Fig. 3.

Fig. 8 shows maps of the modulus of the exact R_{PP} coefficient (top) and of the differences between moduli of first-order and exact R_{PP} coefficients (bottom) for Model B. We can see that the behaviour of the modulus of the exact coefficient is dramatically different from the behaviour of $|R_{PP}|$ in Model A (see upper plot of Fig. 4). We can clearly see the region of rapidly increasing values of $|R_{PP}|$, which indicates critical incidence. As we have already seen in the upper plots of Figs 6 and 7, it extends from angles of incidence of about 75° for azimuths around 0° to angles of incidence of about 50° for azimuths close to 90°. The variation of $|R_{PP}|$ in the overcritical region is negligible in comparison with the variation in the subcritical region. An interesting phenomenon can be observed for small azimuths and angles of incidence ∼50–70°. Along one of the isolines in this region (not shown in the plot), the modulus of the R_{PP} coefficient becomes zero. The angles of incidence along this isoline, which can be seen much better in the bottom plot of Fig. 8 (angles of incidence between 53° and 71° and azimuths between 0° and 16°), represent Brewster angles, for which the reflection

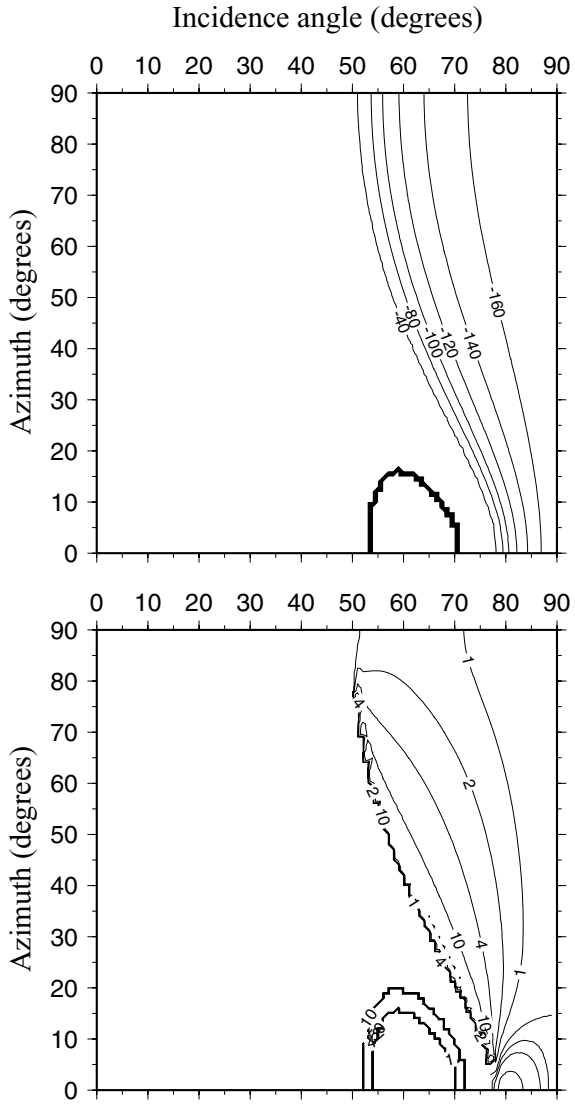

Figure 9. Maps of the phase (in degrees) of the exact R_{PP} coefficient (top) and of the differences between the phases of the first-order and exact R_{PP} coefficients (bottom) for Model B.

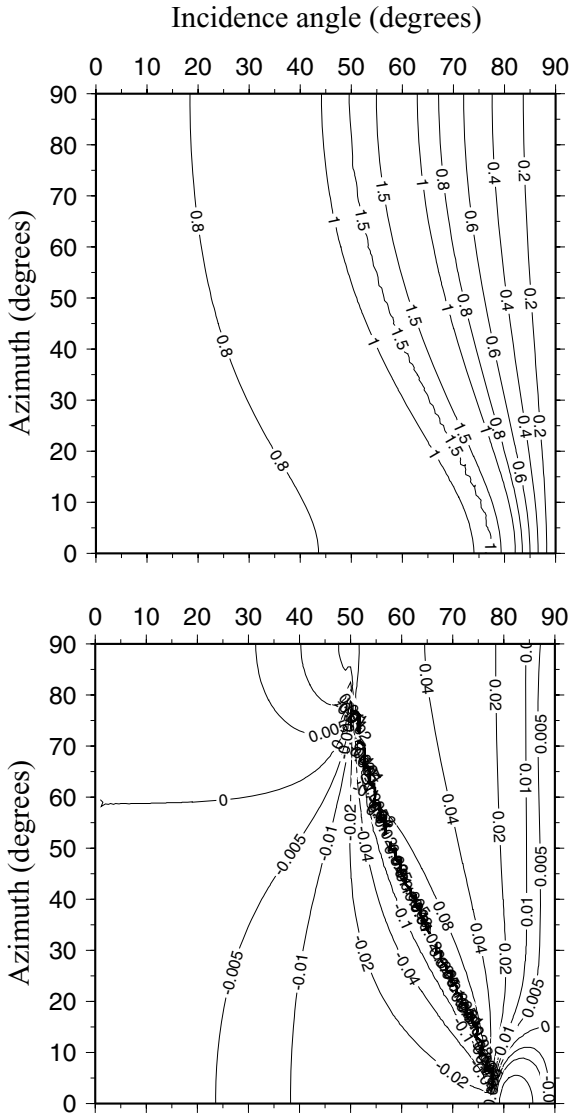

Figure 10. Maps of the moduli of the exact T_{PP} coefficient (top) and of the differences between the moduli of the first-order and exact T_{PP} coefficients (bottom) for Model B.

coefficient is zero. Except for a slight shift of isolines, the map of the modulus of the first-order R_{PP} coefficient (not shown) is nearly identical with the upper plot of Fig. 8. Therefore, the differences shown in the bottom plot of Fig. 8 are generally very small. They only increase significantly in the vicinity of critical incidence and also close to the above-mentioned Brewster angles. The increased density of isolines is the consequence of the slight misposition of the critical and Brewster angles of the approximate coefficients and of the rapid variation of the coefficient in the mentioned regions. Outside these narrow regions, there are no dramatic differences between the approximate and exact coefficients.

For subcritical incidence, the phases, with the exception of the vicinity of the Brewster angles (the isoline between angles of incidence 53° and 71° and between azimuths 0° and 16°), are zero. For overcritical incidence, the phases become non-zero and vary as shown (in degrees) in the upper plot of Fig. 9. At Brewster angles, the phases switch from zero (outside the above-mentioned isoline) to 180° (inside). The differences in phases (in degrees again) shown in the bottom plot indicate that, except for the close vicinity of critical incidence and the Brewster angles (again caused by misposition of the isolines of approximate phases), the approximate phases differ only a little from the exact.

Fig. 10 shows transmission coefficient T_{PP} for Model B. The modulus of the T_{PP} coefficient (top) increases smoothly with the incidence angle up to critical incidence. It then decreases rapidly to zero for tangential incidence. There are no Brewster angles for the T_{PP} coefficient. Although the region of critical incidence in the plot of the modulus of the T_{PP} coefficient is difficult to identify (it is between the isolines of 1.5), it is clearly visible in the plot of differences between approximate and exact moduli of coefficients (bottom). Outside the region of critical incidence, the differences between the first-order and exact moduli are again very small.

As in the case of the reflection coefficient, the phases of the transmission coefficients are zero for subcritical incidence. They become non-zero for overcritical incidence (see the upper plot in Fig. 11) where they are again shown in degrees. Outside the region

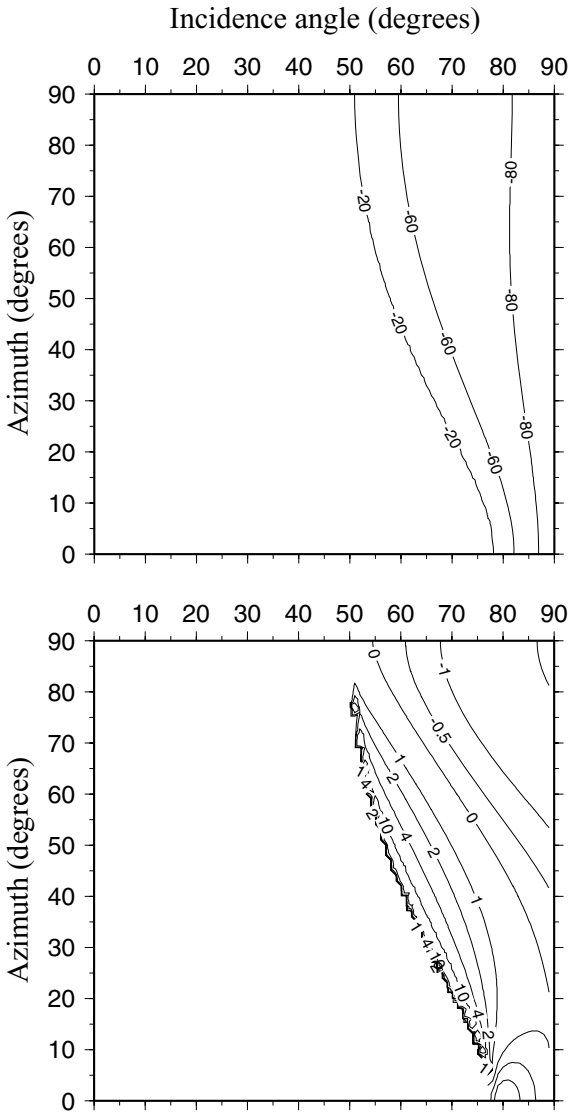

Figure 11. Maps of the phase (in degrees) of the exact T_{PP} coefficient (top) and of the differences between the phases of the first-order and exact T_{PP} coefficients (bottom) for Model B.

of critical incidence, the differences between approximate and exact phases are, as in Fig. 9, very small.

6 CONCLUDING REMARKS

A characteristic and important feature of the first-order coefficients presented in this paper is their applicability to all incidence angles and azimuths. For example, the approximate coefficients of Vavryčuk & Pšenčík (1998), Zillmer *et al.* (1998), Jílek (2002), Rueger (2002) and Klimeš (2003) are applicable only to smaller angles of incidence; they are inapplicable for critical and overcritical reflections and/or transmissions. Another advantage of the approximate coefficients presented in this paper is their applicability to models with arbitrary contrast. The coefficients of the above-mentioned references are applicable only to weak-contrast models. It is also important to emphasize that *S* waves in weakly anisotropic media are considered as one coupled *S* wave in the described first-order R/T coefficients. This was not the case in previous studies of R/T coefficients. The only limitation of the presented coefficients is their restriction to weakly anisotropic media.

The described tests of the first-order R_{PP} and T_{PP} coefficients and related quantities such as slowness and polarization vectors indicate the high accuracy of the approximate formulae. The only exceptions are close vicinities of critical incidence and of the Brewster angles. In applications in ray theory, the inaccuracies of R/T coefficients in the vicinities of critical incidence are not a problem since the ray theory itself does not work properly in these regions.

We plan further tests of more complicated situations, for example, of incidence at an interface separating two weakly anisotropic media, of an incident coupled *S* wave, etc.

ACKNOWLEDGMENTS

A substantial part of this work was done during IP's stay at the IPG Paris at the invitation of the IPGP. We are grateful to reviewers for thorough reviews which helped us to improve the paper considerably. We are also grateful to the Consortium Project 'Seismic waves in complex 3-D structures' (SW3D) and Research Project 205/08/0332 of the Grant Agency of the Czech Republic for support.

REFERENCES

Červený, V., 2001. *Seismic Ray Theory,* Cambridge University Press, Cambridge.

Chapman, C.H., 1994. Reflection/transmission coefficient reciprocities in anisotropic media, *Geophys. J. Int.,* **116,** 498–501.

Chapman, C.H., 2004. *Fundamentals of Seismic Wave Propagation,* Cambridge University Press, Cambridge.

Daley, P.F. & Hron, F., 1977. Reflection and transmission coefficients for transversely isotropic media, *Bull. seism. Soc. Am.,* **67,** 661–675.

Dehghan, K., Farra, V. & Nicolétis, L., 2007. Approximate ray tracing for q*P*-waves in inhomogeneous layered media with weak structural anisotropy, *Geophysics,* **72,** SM47–SM60.

Farra, V. & Pšenčík, I., 2008. First-order ray computations of coupled S waves in inhomogeneous weakly anisotropic media, *Geophys. J. Int.,* **173,** 979–989.

Farra, V. & Pšenčík, I., 2010. Coupled S waves in inhomogeneous weakly anisotropic media using first-order ray tracing, *Geophys. J. Int.,* **180,** 405–417.

Fedorov, F.I., 1968, *Theory of Elastic Waves in Crystals,* Plenum, New York.

Gajewski, D. & Pšenčík, I., 1987. Computation of high-frequency seismic wavefields in 3-D laterally inhomogeneous anisotropic media, *Geophys. J. R. astr. Soc.,* **91,** 383–411.

Graebner, M., 1992. Plane-wave reflection and transmission coefficients for a transversely isotropic solid, *Geophysics,* **57,** 1512–1519.

Jech, J. & Pšenčík, I., 1989. First-order perturbation method for anisotropic media, *Geophys. J. Int.,* **99,** 369–376.

Jílek, P., 2002. Converted PS-wave reflection coefficients in weakly anisotropic media, *Pure appl. Geophys.,* **159,** 1527–1562.

Klimeš, L., 2003. Weak-contrast reflection-transmission coefficients in a generally anisotropic background, *Geophysics,* **68,** 2063–2072.

Musgrave, M.P.J., 1970, *Crystal Acoustics,* Holden-Day, San Francisco.

Pšenčík, I. & Farra, V., 2005. First-order ray tracing for q*P* waves in inhomogeneous weakly anisotropic media, *Geophysics,* **70,** D65–D75.

Pšenčík, I. & Farra, V., 2007. First-order P-wave ray synthetic seismograms in inhomogeneous weakly anisotropic media. *Geophys. J. Int.,* **170,** 1243–1252.

Pšenčík, I. & Vavryčuk, V., 1998. PP wave displacement R/T coefficients in weakly anisotropic media, *PAGEOPH,* **151,** 699–718.

Rueger, A., 1997. P-wave reflection coefficients for transversely isotropic models with vertical and horizontal axis of symmetry, *Geophysics,* **62,** 713–722.

Rueger, A., 2002. *Reflection Coefficients and Azimuthal AVO Analysis in Anisotropic Media,* SEG, Tulsa.

Schoenberg, M. & Protázio, J.S., 1992. Zoeppritz rationalized and generalized to anisotropy, *J. seism. Explor.,* **1,** 125–144.

Ursin, B. & Haugen, G.U., 1996. Weak-contrast approximation of the elastic scattering matrix in anisotropic media, *Pure appl. Geophys.,* **148,** 685–714.

Vanelle, C. & Gajewski, D., 2009. Application of Snell's law in weakly anisotropic media, *Geophysics,* **74,** WB147–WB152.

Vavryčuk, V., 1999. Weak-contrast R/T coefficients in weakly anisotropic elastic media: P-wave incidence, *Geophys. J. Int.,* **138,** 553–562.

Vavryčuk, V. & Pšenčík, I., 1998. PP wave reflection coefficients in weakly anisotropic media, *Geophysics,* **63,** 2129–2141.

Zillmer, M., Gajewski, D. & Kashtan, B.M., 1998, Anisotropic reflection coefficients for a weak-contrast interface, *Geophys. J. Int.,* **132,** 159–166.